

Distribution of HNC O 5₀₅-4₀₄ in Massive Star-forming Regions

Juan Li^{1,2,3}, Junzhi Wang^{1,2}, Qiusheng Gu^{1,2}, and Xingwu Zheng^{1,2}

¹ School of Astronomy & Space Science, Nanjing University, 22 Hankou RD, Nanjing 210093, China e-mail: lijuan@shao.ac.cn

² Key Laboratory of Modern Astronomy and Astrophysics (Nanjing University), Ministry of Education, Nanjing 210093, China

³ Shanghai Astronomical Observatory, CAS, 80 Nandan Road, Shanghai 200030, China

Received 18 December 2012 / Accepted 6 May 2013

ABSTRACT

Aims. The goal of this paper is to study the spatial distribution of HNC O in massive star-forming regions, and investigate its spatial association with infrared sources, as well as physical conditions in region of HNC O emission.

Methods. We have mapped nine massive star-forming regions in HNC O 5₀₅-4₀₄ with the Purple Mountain Observatory 13.7m telescope. The C¹⁸O maps of these sources were obtained simultaneously.

Results. The HNC O emission shows compact distribution, with emission peak centred on water masers. Nearly all the HNC O clumps show signs of embedded mid-infrared or far-infrared sources. The FWHM sizes of HNC O clumps are significantly smaller than C¹⁸O clumps but rather similar to HC₃N clumps. We also found good correlation between the integrated intensities, linewidths and LSR velocities of HNC O and HC₃N emission, implying similar excitation mechanism of these two species. As such, collisional excitation is likely to be the dominant excitation mechanism for HNC O 5₀₅ - 4₀₄ emission in galactic massive star-forming regions.

Key words. ISM: clouds - ISM: molecules - radio lines: ISM

1. Introduction

Interstellar isocyanic acid (HNC O) was first detected in Sgr B2 molecular cloud complex, where it was found to be spatially extended and relatively strong (Snyder & Buhl 1972; Churchwell et al. 1986; Lindqvist et al. 1995; Kuan & Snyder 1996; Dahmen et al. 1997). Since its discovery, HNC O has been detected in various molecular clouds, including the dark cloud TMC-1 (e.g. Brown 1981; Jackson et al. 1984), as well as hot cores in massive star-forming regions (e.g. MacDonald et al. 1996; Helmich & van Dishoeck 1997). Jackson et al. (1984) proposed that HNC O was a dense gas tracer due to coincidence of HNC O emission with regions of high density ($n \geq 10^6 \text{ cm}^{-3}$). Zinchenko et al. (2000) reported a detection rate of 70% in a survey of 81 molecular clouds. HNC O has also been detected in some extragalactic sources (Nguyen-Q-Rieu et al. 1991; Meier & Turner 2005; Martín et al. 2009).

Within the Galactic center region, obvious different distribution of HNC O and C¹⁸O, which is thought to be a tracer of the total H₂ column density, suggests possible different chemical properties of the different molecular complexes in the center of our Galaxy (Dehmen et al. 1997; Lindqvist et al. 1995; Martín et al. 2008). Based on the morphology of the emission and the HNC O abundance with respect to H₂, several authors made the hypothesis that HNC O could be a good tracer of interstellar shocks (e.g., Zinchenko et al. 2000; Meier & Turner 2005; Minh & Irvine 2006). Martín et al. (2008, 2009) conducted a multitransition study of 13 molecular clouds towards the Galactic center and concluded that the HNC O/CS abundance ratio might provide an useful tool in distinguishing between

the influence of shocks and radiation activity in nuclear regions of galaxies. Rodríguez-Fernández et al. (2010) test the hypothesis by observing a low-mass molecular outflow where the chemistry is dominated by shocks. Their results indicate that shocks can actually produce the HNC O abundance measured in galactic nuclei, providing a solid basis to previous suggestions that the extended HNC O in galactic nuclei could trace large scale shocks.

Chemical models have also been developed to investigate how HNC O forms. Both gas-phase reaction (e.g. Turner et al. 1999) and formation routes on grain surfaces (e.g. Hasegawa & Herbst 1993; Garrod et al. 2008) have been used to model HNC O abundance. Tideswell et al. (2010) found that HNC O is inefficiently formed when only gas-phase formation pathways are considered in the chemical network, and surface routes are needed to account for its abundance. Quan et al. (2010) reproduced the abundances of HNC O and its isomers in cold and warm sources using gas-grain simulation, which contains both gas-phase and grain-surface syntheses.

Zinchenko et al. (2000) mapped three molecular clouds in HNC O transitions and found that HNC O emission is compact and centrally peaked. Limited by angular resolutions, the size of HNC O clouds, the relationships with infrared sources, as well as the dominant excitation mechanism of HNC O emission remain unknown. From this consideration it is clear that high-sensitivity observations are needed to better understand the physical condition and chemical properties of HNC O clouds.

In this paper we present large-scale mapping observations of HNC O and C¹⁸O toward strong sources detected in Zinchenko et al. (2000) with the Purple Mountain Ob-

servatory 13.7m (PMODLH 13.7m) telescope. We first introduce the observations and data reduction in § 2. In § 3, we present the observational results. In § 4, we discuss implication of our observations on the excitation mechanism and chemistry of HNC, followed by a summary in § 5.

2. Observations And Data Reductions

We performed mapping observations of HNC $5_{05} - 4_{04}$ (109.905 GHz) and $C^{18}O$ 1-0 (109.782 GHz) lines simultaneously with the PMODLH 13.7m located in Delingha, China in January, 2011. The main beam size of about $55''$ and the pointing accuracy is estimated to be better than $9''$. A new cryogenically cooled 9-beam SIS receiver (3×3 with a separation of $174''$ between the centers of adjacent beams) working in the 85-115 GHz band were employed. A fast Fourier transform spectrometers (FFTS) of 16,384 channels with bandwidth of 1 GHz was used for each beam, supplying a velocity resolution of about 0.21 km s^{-1} . Typical system temperature was around 150-300 K, depending on the weather conditions. Observations were made in on-the-fly mode with nine beams. The telescope is drifting in azimuth (with a rate of $20'' \text{ s}^{-1}$) and stepping in elevation (with a scan step of $15''$). Several maps were made and later combined to lower rms noise levels. The mapping size was $10' \times 10'$ for most sources. Mapping center of all our sources are listed in Table 1.

Most of the sources were selected from dense cores showing strong HNC $5_{05} - 4_{04}$ emission in the surveys of Zinchenko et al. (2000). W44, S140 and DR21S are also included in our sample. W44 is a molecular cloud interacting with a supernovae remnant (SNR), which provides promising environment for production of HNC. Both S140 and DR21S are massive star-forming regions with strong HC_3N emission (Li et al. 2012). Table 1 lists information of the sources that have been mapped in this study. The distances were determined from an extensive literature search. Trigonometric parallax distances were used if available, otherwise photometric distances or kinematic distances based on rotation curve of Fich, Blitz & Stark (1989) were used.

The data processing was conducted using GILDAS package¹. A least-square fit to baselines in the spectra was carried out with the first order polynomial. The baseline slopes were removed for all the sources. The individual spectra were averaged and the resulting spectra were Hanning-smoothed to improve the S/N ratio of the data. The line parameters are obtained by Gaussian fitting. We express the results in the unit of main beam brightness temperature (T_{mb}) assuming the main beam efficiencies of 0.5 (Chen et al. 2010, 2012).

To search for mid-infrared (MIR) emission of young stellar objects (YSOs), we used the *Midcourse Space Experiment* (MSX) Galactic plane survey between 6 and $25 \mu\text{m}$ at $18''$ spatial resolution (Price et al. 2001). For S140, where no MSX data are available, the AKARI/IRC source catalogue (Murakami et al. 2007; Onaka et al. 2007) of AKARI all sky survey is used to search for MIR emission (9 and $18 \mu\text{m}$) with spatial resolution of about $6''$. To search for far-infrared (FIR) emission of YSOs, we used AKARI/FIS bright source catalogue (Kawada et al. 2007) centered at 65, 90, 140 and $160 \mu\text{m}$, with spatial resolutions range from $37''$ to $61''$.

¹ <http://www.iram.fr/IRAMFR/GILDAS>.

3. Observing Results

Figure 1 presents the HNC $5_{05} - 4_{04}$ and $C^{18}O$ 1-0 spectra of S140 and W44. Both of them are newly detected in HNC. The derived line parameters of HNC $5_{05} - 4_{04}$ and $C^{18}O$ 1-0 at (0, 0) are presented in Table 2 and 3, respectively, including main beam brightness temperature (T_{mb}), integrated line intensity ($\int T_{mb} d\nu$), LSR velocity and full-width half-maximum (FWHM) linewidth of HNC $5_{05} - 4_{04}$ emission. All the parameters are determined from Gaussian fitting. Our derived parameters are similar but not identical to results of Zinchenko et al. (2000) because their main beam size is only two-thirds of our observations.

HNC $5_{05} - 4_{04}$ maps were obtained for nine sources. In Figure 2 and 3, we present contour maps of HNC $5_{05} - 4_{04}$ (solid lines) and $C^{18}O$ (dashed lines) overlaid on MSX $21.3 \mu\text{m}$ image in linear scale. Except Orion KL, other eight sources have been mapped with the same telescope and toward the same positions with HNC in HC_3N 10-9 transition (90.979 GHz) (Li et al. 2012). The HC_3N contour maps (dotted lines) were also overlaid for comparison. The MIR and FIR sources from AKARI catalogues are marked by asterisk (*) and star (★), respectively. Red filled squares are used to mark positions of water masers. Compared with the widespread $C^{18}O$ distribution, HNC emission shows rather compact distribution, with emissions well concentrating on water masers. The HNC emission peaks offset from the $C^{18}O$ in Orion A, W51M and S158. Recently improved resolution of infrared observations allow us to better understand the relationship between HNC clumps and infrared sources. Nearly all the HNC clumps are spatially coincident with MIR or FIR sources, which usually trace the warm dust emission of the cocoons of the OB star central exciting sources. The morphology and spatial distribution of HNC $5_{05} - 4_{04}$ emission are similar to HC_3N 10-9 transition, which is a dense gas tracer (e.g. Li et al. 2012). These results imply that HNC emission is emitted from a small volume of warmer and denser gas located nearer to the embedded objects than the $C^{18}O$ emission.

The size of clouds is characterized using beam deconvolved angular diameter and linear radius of a circle with same area as the half peak intensity:

$$\theta_{transition} = 2 \left(\frac{A_{1/2}}{\pi} - \frac{\theta_{beam}^2}{4} \right)^{1/2}, \quad (1)$$

$$R_{transition} = D \left(\frac{A_{1/2}}{\pi} - \frac{\theta_{beam}^2}{4} \right)^{1/2}, \quad (2)$$

where $A_{1/2}$ is the area within the contour of half peak intensity, θ_{beam} is the FWHM beam size, and D is the distance of the source. The deconvolved linear FWHM sizes and angular diameter of HNC and $C^{18}O$ clouds are presented in Table 2 and 3, respectively. The deconvolved linear sizes of HNC clouds range from 0.05 to 2.88 pc, with the smallest value comes from Orion KL, and the largest value comes from W51M. The sizes of HNC clouds are significantly smaller than those of $C^{18}O$ for nearly all the sources except W75OH, in which the size of HNC cloud is comparable to that of $C^{18}O$.

Below we give comments on individual sources.

G121.30+0.66. We detected HNC $5_{05} - 4_{04}$ emission with T_{mb} of 0.24 K. The HNC clump has a centrally condensed structure, with emission peak coincides with the MIR emission.

Orion KL. Orion KL is the closest massive star-forming region (414 pc; Menten et al. 2007). Several molecular components, such as the Hot Core, Compact and Extended Ridges, and several luminous IR sources or radio sources are associated with Orion KL. The nature of the sources responsible for the luminous IR emission is still poorly known and much debated. Other than being powered by an embedded central heating source (e.g., Kaufman et al. 1998), an interesting alternative explanation for this region's energetics is a protostellar merger event that released a few times 10^{47} erg of energy about 500 years ago (Bally & Zinnecker 2005; Zapata et al. 2011; Bally et al. 2011). Our observations show that the HNC peak displace from the $C^{18}O$ peak and is centered on *MSX* 21.3 μm emission peak. The HNC/ $C^{18}O$ intensity ratio at (0, 0) is close to unity, while they are less than 0.25 in other sources. As shock enhancement of HNC has been detected in L1157 molecular outflow (Rodríguez-Fernández et al. 2010), the relatively high HNC/ $C^{18}O$ intensity ratio seem to favor the idea that the chemistry in Orion KL should be shock driven with much higher temperature than the chemistry in a typical hot core (Favre et al. 2011), and produce high abundances of HNC (Zinchenko et al. 2000).

W44. W44 is a SNR with shell-like morphologies (Dubner et al. 2000; Jones et al. 1993). It locates adjacent to giant molecular cloud with which it is suspected to be interacting (Wootten 1981; Denoyer 1983). It contains OH 1720 MHz masers attributed to dense shocked gas (Lockett et al. 1999). The *MSX* image of W44 consists of a SNR and dust emission heated by embedded YSOs. If it is correct that HNC is enhanced in the presence of shocks due to its injection in the gas phase from the grain mantles (Zinchenko et al. 2000), HNC would be expected in molecular clouds interacting with SNRs. Strong HNC emission was detected with T_{mb} of 0.58 K. The HNC emission mainly concentrates around the YSO. More sources should be observed to investigate whether HNC is abundant in molecular clouds interacting with SNRs.

W51M. This is a strong HNC $5_{05-4_{04}}$ emission source with T_{mb} of 0.48 K. Two cores were seen in HNC clouds. The western peak, W51m-west, is stronger than the eastern peak in HNC emission, but weaker than the eastern peak in HC_3N and $C^{18}O$ emission. W51m-west is centered on the *AKARI* FIR sources, while the eastern peak is coincident with water masers and near to MIR sources.

ON1. We detected HNC $5_{05-4_{04}}$ emission with T_{mb} of 0.22 K. Similar to G121.30+0.66, the HNC emission morphology has a centrally condensed structure, with the emission peak coincides with the MIR emission.

DR21S. DR21S is a strong HC_3N emission source in Li et al. (2012). This is a massive clump in the Cygnus X region. HNC was detected in DR21S with T_{mb}^* of 0.12 K. The HNC emission peak is near to the MIR emission peak position.

W75OH. W75OH is also a massive clump in the Cygnus X region, which hosts three massive dense cores at an early stage of their evolution. We detected HNC $5_{05-4_{04}}$ emission with T_{mb} of 0.38 K. Two HNC cores were seen in W75OH. The southern peak is brighter than the northern peak in HNC emission. The southern peak is near to the *AKARI* FIR source, while the northern clump, W75OH-north, is near to the strong MIR emission. Csengeri et al. (2011) reported detection of velocity shears and low-velocity shocks in W75OH. Since HNC is thought to be

enhanced by low-velocity shocks, high resolution observations of this source is expected to test this hypothesis by comparing the spatial distribution of HNC and N_2H^+ convergent flows.

S158. S158 is also referred as NGC7538 (Moreno & Chavarría-K 1986). We detected HNC $5_{05-4_{04}}$ emission with T_{mb} of 0.44 K. Two clumps were seen in HNC and HC_3N clouds, with the stronger one coincident with the *AKARI* MIR source.

S140. S140 shows strong HC_3N emission in Li et al. (2012). HNC $5_{05-4_{04}}$ was marginally detected with T_{mb} of 0.16 K. Two HNC cores were seen with low signal-to-noise ratio. One of them is associated with the *AKARI* MIR sources, while another one is starless.

4. Discussions

Churchwell et al. (1985) mapped 14 transitions of HNC toward Sgr B2. Analysis of population distribution indicates the FIR radiation from warm dust is likely to be responsible for the excitation of HNC. They proposed that the most likely excitation mechanism of HNC in Sgr B2 was radiative rather than collisional. In this case HNC was a good probe of the FIR radiation field but not of gas properties such as density and kinetic temperature. The physical environment of hot cores differ from the Galactic center, in which the gas density (10^3 - 10^4 cm^{-3}) is much lower than in hot cores, thus the dominant excitation mechanism might be different. Zinchenko et al. (2000) explained the $K_{-1} > 0$ ladders of Orion KL with radiative excitation. For the $K_{-1} = 0$ transitions with larger source size, Zinchenko et al. (2000) proposed that the radiative excitation would become inefficient, and the collisional excitation may dominate.

In Figure 4, we present plots comparing integrated intensities, linewidths, FWHM size and LSR velocities of HNC $5_{05-4_{04}}$ and HC_3N 10-9 (Li et al. 2012)². The source names are also labeled in the figure. Good correlation is found for integrated intensities ($r_{corr} = 0.63$) and FWHM sizes ($r_{corr} = 0.98$) of HNC and HC_3N clumps. The linewidths of HNC clumps also agree well with HC_3N clumps ($r_{corr} = 0.92$), with the only exception of S140, which is possibly caused by the marginal detection of HNC ($< 3\sigma$) in this source (see Figure 1). The velocity difference between HNC and HC_3N are within 3σ for all sources except W51M, which is possibly related to the complex structure of this source. The obvious correlations between line parameters as well as the similar morphology of HNC and HC_3N clumps suggest that these two molecule lines are tracing a similar volume of gas. The critical density of HC_3N 10-9 is 10^6 cm^{-3} (e.g., Chung et al. 1991), which is comparable with the critical density of HNC $5_{05-4_{04}}$. The dominant excitation mechanism for HC_3N is collisional excitation, thus collisional excitation is likely to be the dominant excitation mechanism for HNC $K_{-1} = 0$ emission in galactic massive star-forming regions.

In sources mapped by Zinchenko et al. (2000), HNC emission peaks are significantly displaced from any known IR sources. However, observations at that time were severely limited by resolution of infrared observations. With greatly improved spatial resolution and sensitivity of

² We obtain T_{mb} of HC_3N by assuming the main beam efficiencies of 0.5.

IR observations, we found that nearly all the HNC₂O clumps in our observations are associated with MIR or FIR emission. Thus HNC₂O should be produced in hot gas. This is consistent with Bisschop et al. (2007), in which HNC₂O was classified as "hot" molecules based on rotation diagram analysis. Sanhueza et al. (2012) observed a sample of infrared dark clouds (IRDCs) and found that HNC₂O profiles show no evidence of being a tracer of shocks in most of the sources, only in two sources, which represent 10% of the sources with HNC₂O detection, the HNC₂O spectrum presents a blue wing that is also observed in SiO. For results present here, we found possible shock enhancement of HNC₂O in two sources (Orion KL and W75OH). We conclude that HNC₂O is produced in warm environment, while shock could enhance the HNC₂O abundance.

5. Summary and Prospects

In this paper we present HNC₂O 5₀₅ – 4₀₄ mapping observations of nine massive star-forming regions with the PMODLH 13.7m telescope. The C¹⁸O 1-0 maps of these sources are obtained simultaneously. We used *MSX* and *AKARI* satellite data to search for infrared emission from YSOs and investigate the spatial relationship between HNC₂O clumps and infrared sources.

We found good correlations between line parameters of HNC₂O and HC₃N emission, implying similar excitation mechanism of these two molecules. The size of HNC₂O clumps are much smaller than the C¹⁸O clumps and comparable with the HC₃N clumps. Thus collisional excitation is likely to be the dominant excitation mechanism for HNC₂O 5₀₅-4₀₄ transition in galactic massive star-forming regions.

We found that HNC₂O emission is compact and centrally condensed. Nearly all the HNC₂O clumps show signs of embedded infrared emission, supporting the idea that HNC₂O is a "hot" molecules. Future high resolution observations of W75OH is expected to test the hypothesis that HNC₂O is enhanced by low-velocity shock by comparing the spatial distribution of HNC₂O and N₂H⁺ convergent flows.

PMO is carrying out CO, ¹³CO and C¹⁸O 1-0 survey toward the Galactic plane with the DLH 13.7m telescope. HNC₂O 5₀₅-4₀₄ could be observed simultaneously within the 1 GHz band, which would enable us to obtain spatial distribution of strong HNC₂O emission in the Galactic plane and better study the chemical properties of HNC₂O.

Acknowledgements. We thank the referee for his/her helpful comments and constructive suggestions. This work is partly supported by China Ministry of Science and Technology under State Key Development Program for Basic Research (2012CB821800), and partly supported by the Natural Science Foundation of China under grants of 11103006, 10833006 and 10878010. We would like to thank Key Laboratory of Radio Astronomy, Chinese Academy of Sciences. We are very grateful to the staff of Qinghai Station of Purple Mountain Observatory for their assistance with the observations and data reductions. This research made use of data products from the *Midcourse Space Experiment*. This research is based on observations with *AKARI*, a JAXA project with the participation of ESA. This research has made use of the NASA/IPAC Infrared Science Archive, which is operated by the Jet Propulsion Laboratory, California Institute of Technology, under contract with the National Aeronautics and Space Administration.

References

Bally, J. Cunningham, N. J., Moeckel, N. et al. 2011, ApJ, 727, 113
Bally, J. & Zinnecker, H. 2005, AJ, 129, 2281

Bisschop, S. E., Jorgensen, J. K., van Dishoeck, E. F. & de Wachter, E. B. M. 2007, A&A, 465, 913
Brown, R. L. 1981, ApJ, 248, 119
Chen, X., Shen, Z.-Q., Li, J. J. et al. 2010, ApJ, 710, 150
Chen, X., Ellingsen, S. P., He, J.-H. et al. 2012, ApJS, 200, 5
Chung, H. S., Kameya, O. & Morimoto, M. 1991, JKAS, 24, 217
Churchwell, E., Wood, D., Myers, P. C. & Myers, R. V., 1986, ApJ, 305, 405
Csengeri, T., Bontemps, S., Schneider, N. et al. 2011, ApJ, 740, 5
Dahmen, G. et al. 1997, A&AS, 126, 197
Denoyer, L. K. 1983, ApJ, 264, 141
Dubner, G. M., Velaázquez, P. F., Goss, W. M. & Holdaway, M. A. 2000, AJ, 120, 1933
Favre, C., Despois, D., Brouillet, N. et al. 2011, A&A, 532, 32
Fich, M., Blitz, L., Stark, A. A. 1989, ApJ, 342, 272
Garrod, R. T., Weaver, S. L. W. & Herbst, E. 2008, ApJ, 682, 283
Hasegawa, T. I. & Herbst, E. 1993, MNRAS, 261, 83
Helmich, F. P. & van Dishoeck, E. F. 1997, A&AS, 124, 205
Jackson, J. M., Armstrong, J. T. & Barrett, A. H. 1984, ApJ, 280, 608
Jones, L. R. Smith, A. & Angellini, L. 1993, MNRAS, 265, 631
Kawada, M., Baba, H., Barthel, P. D. et al. 2007, PASJ, 59, 389
Kaufman, M. J., Hollenbach, D. J. & Tielens, A. G. G. M. 1998, ApJ, 497, 276
Kuan, Y. J., Snyder, L. E. 1996, ApJ, 470, 981
Li, J., Wang, J. Z., Gu, Q. S., Zhang, Z.-Y. & Zheng, X. W. 2012, ApJ, 745, 47
Lindqvist, M., Sandqvist, A., Winnberg, A., Johansson, L. E. B. & Nyman, L.-A. 1995, A&AS, 113, 257
Lockett, P., Gauthier, E. & Elitzur, M. 1999, ApJ, 511, 235
MacDonald, G. H., Gibb, A. G., Habing, R. J. & Millar, T. J. 1996, A&AS, 119, 333
Martin, S., Requena-Torres, M. A., Martin-Pintado, J. & Mauersberger, R. 2008, ApJ, 678, 245
Martin, S., Martin-Pintado, J. & Mauersberger, R. 2009, ApJ, 694, 610
Meier, D. S., & Turner, J. L., 2005, ApJ, 618, 259
Menten, K. M., Reid, M. J., Forbrich, J. & Brunthaler, A. 2007, A&A, 474, 515
Minh, Y. C. & Irvine, W. M. 2006, NewA, 11, 59
Moreno, M. A. & Chavarría-K, C. 1986, A&A, 161, 130
Murakami, H. et al. 2007, PASJ, 59, 369
Nguyen-Q-Rieu, H., Henkel, C., Jackson, J. M., Mauersberger, R. 1991, A&A, 241, 33
Onaka, T., Matsuhara, H., Wada, T. et al. 2007, PASJ, 59, 401
Price, S. D., Egan, M. P., Carey, S. J. et al. 2001, AJ, 121, 2819
Quan, D. H., Herbst, E., Osamura, Y. & Roueff, E. 2010, ApJ, 725, 2101
Rodríguez-Fernández, N. J., Tafalla, M., Gueth, F. & Bachiller, R., 2010, A&A, 516, 98
Sanhueza, P., Jackson, J. M., Foster, J. B. et al. 2012, ApJ, 756, 60
Snyder, L. E. & Buhl, D. 1972, ApJ, 177, 619
Tideswell, D. M., Fuller, G. A., Millar, T. J. & Markwick, A. J. 2010, A&A, 510, 85
Turner, B. E., Terzieva, R. & Herbst, E. 1999, ApJ, 518, 699
Wootten, A. 1981, ApJ, 245, 105
Zapata, L. A., Schmid-Burgk, J. & Menten, K. M. 2011, A&A, 529, 24
Zinchenko, I., Henkel, C. & Mao, R. Q. 2000, A&A, 361, 1079

Table 1. Source List.

source name	RA(J2000)	DEC(J2000)	D (kpc)	Ref.
G121.30+0.66	00:36:47.51	63:29:02.1	1.2	1
Orion KL	05:35:14.47	-05:22:27.56	0.414	2
W44	18:53:18.50	01:14:56.7	3.7	3
W51M	19:23:43.86	14:30:29.4	5.41	4
ON1	20:10:09.14	31:31:37.4	2.57	5
DR21S	20:39:00.80	42:19:29.8	1.5	6
W75OH	20:39:01.01	42:22:49.9	1.5	6
S158	23:13:44.84	61:26:50.71	2.65	7
S140	22:19:19.04	63:18:50.4	0.76	8

References: (1) Plume et al. 1992; (2) Menten et al. 2007; (3) Solomon et al. 1987;; (4) Sato et al. 2010; (5) Rygl et al. 2010; (6) Rygl et al. 2011; (7) Moscadelli et al. 2009; (8) Hirota et al. 2008.

Table 2. Observational results of HNC O 5₀₅-4₀₄ Transition.

Source Name	T_{mb} (K)	$\int T_{mb} d\nu$ (K km s ⁻¹)	V_{LSR} (km s ⁻¹)	FWHM (km s ⁻¹)	$R_{HNC O}$ (pc)	$\theta_{HNC O}$ (arcsec)
G121.30+0.66	0.24(.04)	0.62(.08)	-17.09(.13)	2.36(.40)	0.17	28
Orion KL	0.96(.12)	7.10(.26)	7.94(.11)	5.99(.34)	0.03	11
W44	0.58(.08)	3.24(.22)	58.27(.16)	5.20(.46)	0.67	37
W51M	0.48(.06)	4.80(.22)	55.75(.22)	9.52(.51)	1.44	55
W51M-west	0.46(.06)	5.46(.22)	64.58(.23)	11.28(.48)	-	-
ON1	0.22(.06)	1.12(.12)	11.79(.26)	4.63(.59)	0.45	36
DR21S	0.12(.03)	0.46(.06)	-2.17(.21)	3.50(.56)	0.29	39
W75OH-north	0.26(.04)	1.04(.10)	-3.25(.17)	3.75(.46)	-	-
W75OH	0.38(.04)	1.60(.10)	-3.31(.13)	4.02(.32)	0.50	68
S158	0.44(.06)	1.96(.12)	-56.15(.13)	4.23(.29)	0.69	53
S140	0.16(.06)	1.08(.16)	-7.10(.47)	6.03(1.21)	0.15	41

Table 3. Observational results of C¹⁸O 1-0 Transition

Source Name	T_{mb} (K)	$\int T_{mb} d\nu$ (K km s ⁻¹)	V_{LSR} (km s ⁻¹)	FWHM (km s ⁻¹)	$R_{HNC O}$ (pc)	$\theta_{HNC O}$ (arcsec)
G121.30+0.66	1.52(.06)	3.32(.06)	-17.33(.02)	2.04(.05)	0.43	73
Orion KL	1.76(.08)	7.72(.14)	8.84(.04)	4.13(.10)	0.16	78
W44	4.42(.08)	26.66(.26)	58.19(.03)	5.68(.07)	1.40	78
W51M	2.70(.08)	31.94(.06)	56.49(.06)	11.10(.11)	2.20	84
W51M-west	1.21(.08)	25.34(0.40)	60.90(.16)	19.66(.34)	-	-
ON1	1.78(.06)	6.70(.12)	11.35(.03)	3.53(.07)	0.74	59
DR21S	2.92(.06)	9.60(.10)	-2.37(.01)	3.09(.04)	0.52	71
W75OH-north	3.22(.04)	9.66(.08)	-3.69(.01)	2.82(.03)	-	-
W75OH	2.06(.04)	11.22(.12)	-2.95(.02)	3.45(.04)	0.63	87
S158	1.38(.10)	7.98(.20)	-56.18(.07)	5.43(.17)	1.27	98
S140	2.08(.06)	6.54(.14)	-7.23(.03)	2.95(.07)	0.40	108

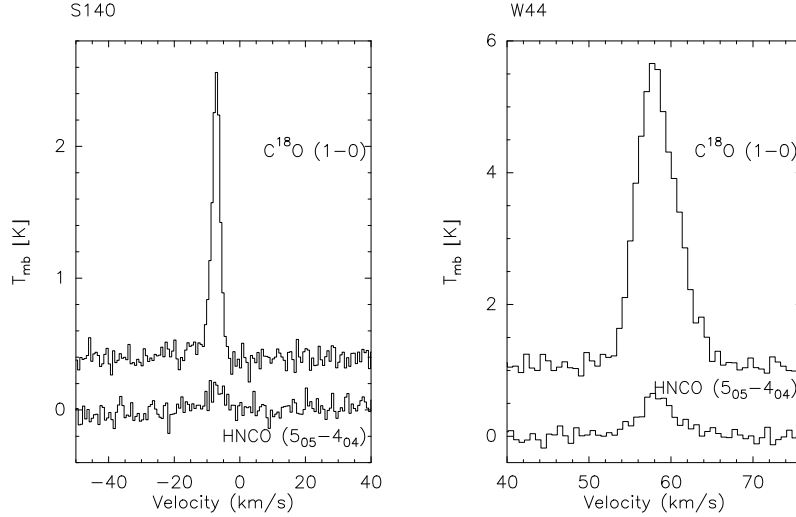


Fig. 1. HNC O 5₀₅-4₀₄ and C¹⁸O 1-0 spectra of S140 and W44 at (0, 0). The identification of the transitions is given to the right of each lines.

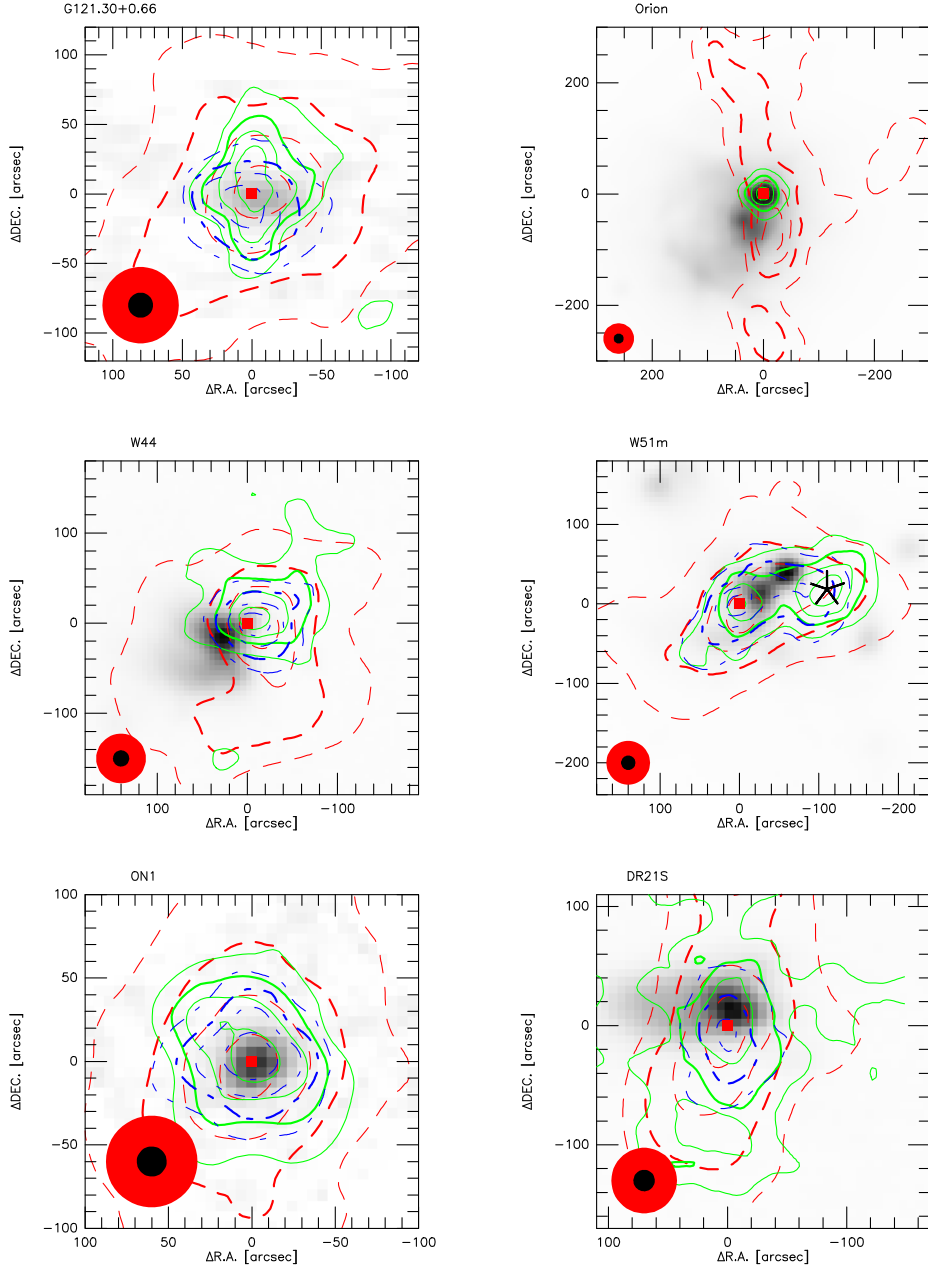


Fig. 2. Contour maps of HNC (green solid line), HC₃N (blue dotted line) and C¹⁸O (red dashed line) superimposed on *MSX* 21.3 μ m image for observing sources. The contour levels are 30%, 50%, 70% and 90% of the map peak, reported in Table 3 (see Column 3 for HNC, Column 7 for C¹⁸O, see Column 3 in Table 3 of Li et al. (2012) for HC₃N). The heavy lines represent 50% of the map peak. "*" is used to mark the position of the *AKARI* FIR source. "*" is used to mark the position of the *AKARI* MIR source in S140. Red filled squares are used to mark the position of water masers. The FWHM beam size for molecular lines (the big, red circle) and mid-infrared (the small, black circle) observations are shown at the lower left the maps. (A color version of this figure is available in the online journal.)

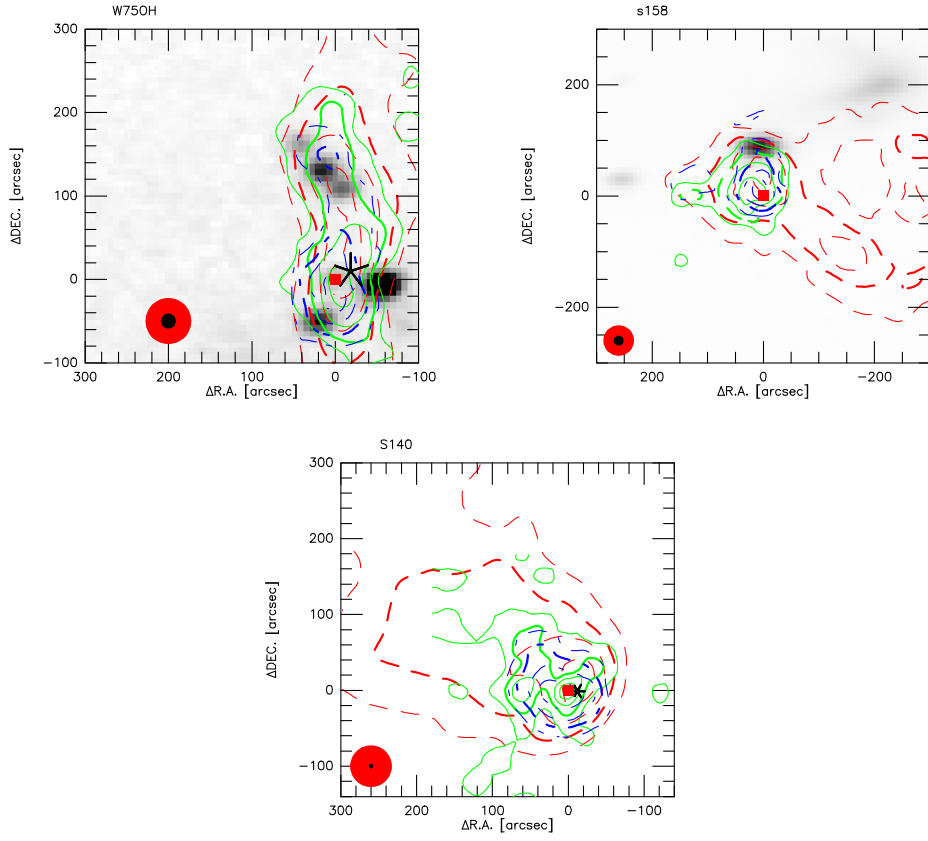


Fig. 3. Figure 2 continued. (A color version of this figure is available in the online journal.)

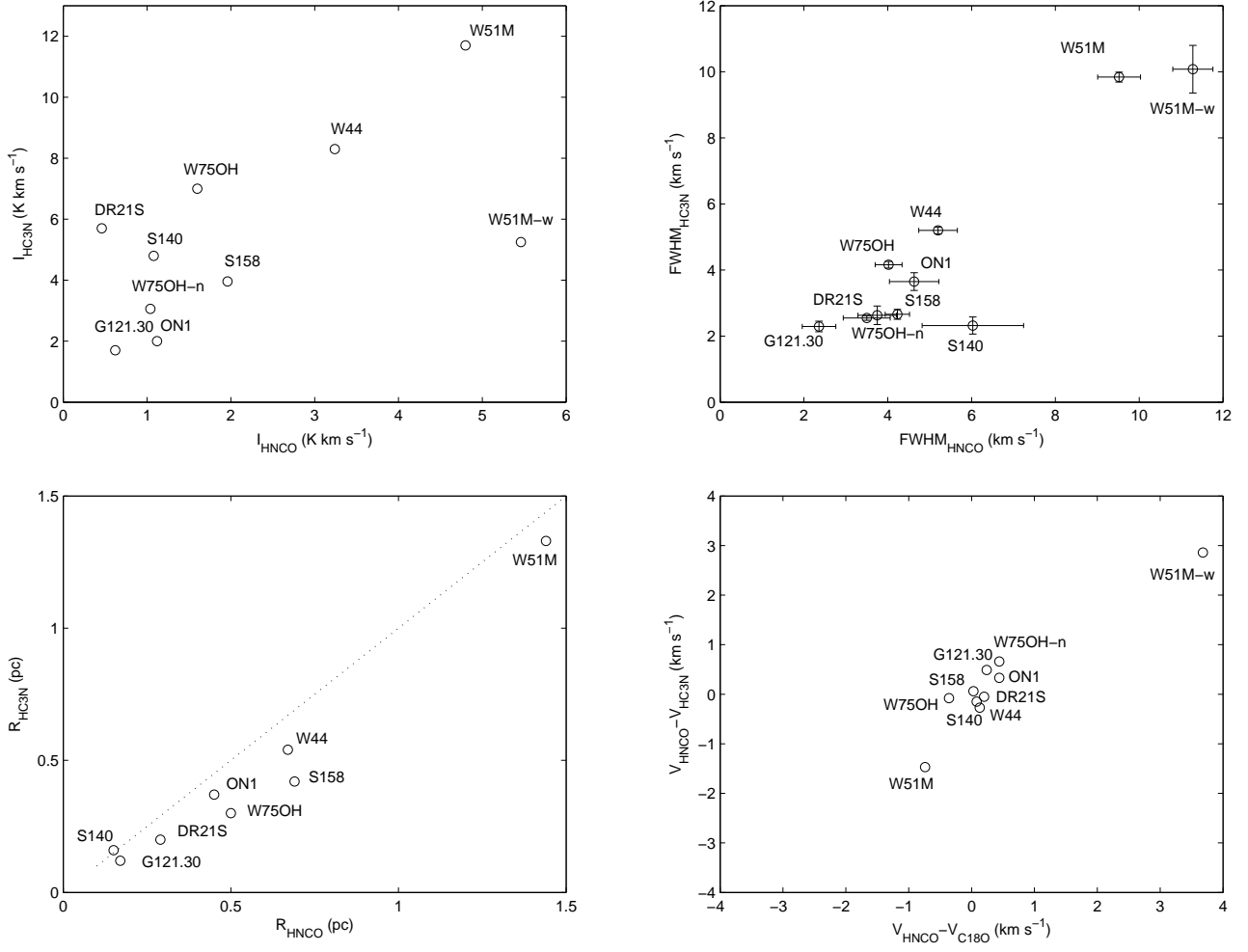


Fig. 4. Upper left: comparison of integrated intensities of HNC $5_{05}-4_{04}$ and HC₃N 10-9; upper right: comparison of linewidth of HNC $5_{05}-4_{04}$ and HC₃N 10-9; lower left: comparison of size of HNC $5_{05}-4_{04}$ and HC₃N 10-9. The dotted line has a slope of 1; lower right: LSR velocity difference between HNC $5_{05}-4_{04}$ and HC₃N 10-9 versus LSR velocity difference between HNC $5_{05}-4_{04}$ and C¹⁸O 1-0. The source names were also labeled in the figure.

